Al-Azhar Engineering 16th International Conference

Vol. 19, No. 72, July 2024, 147 - 161

PERFORMANCE COMPARATIVE STUDY OF LOW REYNOLDS NUMBER AIRFOILS UTILIZED IN VERTICAL-AXIS WIND TURBINES

M. Shaaban Abul-Ela[1*], Ashraf I. Sayed[2], M. Elfaisal Elrefaie[3]

[1*]Mechanical Power Engineering Department, Faculty of Engineering, Ahram Canadian University, 12451, Giza, Egypt
[2]Mechanical Power Engineering Department, Faculty of Engineering, Cairo University, 12613, Giza, Egypt
[3]Mechanical Power Engineering Department, Faculty of Engineering, Al-Azhar University, Nasr City, 11884, Cairo, Egypt
*Correspondence: muhammadshaaban92@gmail.com

Citation:

M.S. Abul-Ela, A.I. Sayed and M.E. Elrefaie, "Performance comparative study of low Reynolds number airfoils utilized in vertical-axis wind turbines", Journal of Al-Azhar University Engineering Sector, vol. 19, pp. 147 161, 2024.

Received: 24 December 2023

Revised: 07 February 2024

Accepted: 18 February 2024

DOI:10.21608/auej.2024.257724.1548

ABSTRACT

Recently, utilizing wind power has increased thanks to its cleanness, cheapness, and wide availability. In many countries, the dependency on wind power has become enormous and vital in industry. Consequently, the improvement of the wind turbine's aerodynamic performance is a crucial issue according to Egypt Vision 2030 for using new and renewable energy resources. Vertical-axis wind turbines (VAWTs) are an appropriate solution in low-wind speed areas owing to their small size and ease of manufacturing. This paper presents a qualitative and quantitative comparative analysis of the aerodynamic performance of various low-Reynolds number airfoils of a small-scale, three-straight-bladed H-rotor vertical-axis wind turbine. The examined airfoils are NACA0021 (as a reference model), NACA6712, Eppler474, S1210, S1048, and DU-06-W-200 at tip-speed ratios (TSRs) ranging from 1.2 to 4.0. For the chosen airfoils, the maximum power coefficient and its corresponding tip-speed ratio were studied. ANSYS Fluent was used to execute 2D CFD simulations using the SST-k-ω turbulence model to solve Unsteady Reynolds-Averaged Navier-Stokes (URANS) equations. The maximum power coefficient of the reference model, NACA0021, was approximately 0.3263 at TSR = 2.63. The results revealed that the NACA6712 airfoil possessed the best aerodynamic performance at low tip-speed ratios (from 1.2 to 2.4). It experienced a percentage improvement in power coefficient of about 12% at TSR = 2.037 relative to the reference model. In addition, the Eppler474 airfoil performed efficiently for almost all TSRs' ranges, specifically high TSRs. Its power coefficient was enhanced by about 9% at TSR = 3.0 relative to the reference model.

KEYWORDS: Darrieus Turbine, Airfoils, Vertical-Axis Wind Turbine, Low Reynolds number flow, ANSYS Fluent, CFD, Unsteady Aerodynamics.

دراسة مقارِنة لأداء الجُنَيّحات ذات عدد رينولدز المنخفض المستخدمة في تربينات الرياح ذات المحور الرأسي

محمد شعبان أبو العلا[1*]، أشرف إبراهيم سيد[2]، محمد الفيصل الرفاعي[3]

[1]قسم الهندسة الميكانيكية، كلية الهندسة، جامعة الأهرام الكندية، مدينة السادس من أكتوبر، مصر.
[2]قسم هندسة القوى الميكانيكية، كلية الهندسة، جامعة القاهرة، الجيزة، مصر.
[3]قسم هندسة القوى الميكانيكية، كلية الهندسة، جامعة الأزهر، مدينة نصر، 11884، القاهرة، مصر
*البريد الاليكتروني للباحث الرئيسي: muhammadshaaban92@gmail.com

الملخص

في الآونة الأخيرة، ازداد استخدام طاقة الرياح بفضل نظافتها، ورُخْص ثمنها، وتوافرها على نطاق واسع. في العديد من البلدان، أصبح الاعتماد على طاقة الرياح هائلًا وحيويًّا في الصناعة، وبالتالي فإن تحسين الأداء الديناميكي الهوائي لتربينات الرياح يُعَد أمرًا بالغ الأهمية وفقًا لرؤية مصر 2030 لاستخدام موارد الطاقة الجديدة والمتجددة، وتُعَد تربينات الرياح ذات المحور الرأسي (VAWTs) حلًّا مناسبًا في المناطق ذوات سرعات الرياح المنخفضة؛ نظرًا لصغر حجمها وسهولة تصنيعها. يقدم هذا البحث تحليلًا مُقارِنًا نوعيًّا وكميًّا للأداء الديناميكي الهوائي لمختلِف الجُنَيّحات العاملة عند عدد رينولدز المنخفض لتربينات رياح صغيرة الحجم ذات ثلاث شفرات مستقيمة من النوع H. تم فحص الجُنَيّحات الآتية: NACA0021 بوصفه نموذجًا مرجعيًّا، وNACA6712، وEppler474، وS1210، وS1048، وDU-06-W-200 عند نسب سرعة الطرَف (TSRs) التي تمتد من 1.2 إلى 4.0. وبالنسبة للجُنَيّحات المختارة، فقد تم دراسة معامل القدرة الأقصى ونسبة سرعة الطرَف المناظرة له. تم استخدام ANSYS Fluent لتنفيذ عمليات محاكاة CFD الثنائية الأبعاد باستخدام نموذج الاضطراب SST-k-ω لحل معادلات Unsteady-Reynolds-Averaged Navier-Stokes (URANS). بلغ معامل القدرة الأقصى للنموذج المرجعي NACA0021 نحو 0.3263 عند نسبة سرعة الطرَف 2.63. وقد أظهرت النتائج أن الجُنَيّح NACA6712 ذو أداء ديناميكي هوائي أفضل عند نسب سرعة الطرَف المنخفضة (من 1.2 إلى 2.4)، وقد نتج عنه تحسن في معامل القدرة بنسبة مئوية بنحو 12% عند نسبة سرعة الطَرَف 2.037 مقارنةً بالنموذج المرجعي. فضلًا عن ذلك، كان أداء الجُنَيّح Eppler474 مُحَسَّنًا في جميع نطاقات نسب سرعة الطرَف تقريبًا، لا سيما عند نسب سرعة الطَرَف العالية، وتم تعزيز معامل القدرة الخاص به بنحو 9% عند نسبة سرعة الطرَف 3.0 مقارنةً بالنموذج المرجعي.

الكلمات المفتاحية: توربين داريوس، الجنيحات، توربينات الرياح ذات المحور الرأسي، تدفق عدد رينولدز المنخفض، ANSYS Fluent، CFD، الديناميكا الهوائية غير المستقرة.

1. Introduction

Wind turbines are popular energy-harvesting devices that generate electricity from wind energy. Small wind turbines are used on building roofs, farms isolated urban areas, and boats [1]. Installation of the vertical axis wind turbines (VAWTs) is suitable in low-wind speed areas.[2]. One of the most significant parameters used to characterize the flow and crucial in airfoil shape selection is the Reynolds number “Re”. Low-Reynolds number airfoils are depicted in [3], and [4].

At low Reynolds numbers, some aerodynamic issues might arise, such as Laminar Separation Bubbles (LSBs) [5]. They might be formed on the surface of the airfoil and result in decreasing its performance, ultimately causing it to stall due to an abrupt drop in lift and an increase in drag specifically for Reynolds number below 50,000 [6].

T. Tahzib et al. [7] studied numerically a three-bladed H-Darrius wind turbine performance using two different symmetric airfoils; NACA0018 and S1046. The analysis focused on the effect of blade angle and tip speed ratio. The results showed that the S1046 with -2° pitch angle and operating at $\lambda = 4.0$ was the better choice for low and unstable wind speed areas. The best performance of a certain VAWT was explored by Roy and Branger [8] after studying a variety of NACA and S blade airfoil profiles while considering the number of blades, aspect ratio, and solidity ratio. However, neither the pitch angle impact nor the TSR was examined. Hashem et al. [9] utilized the S1046 airfoil and provided a wind lens for enhancing the VAWT aerodynamic performance. Despite the study of massive shapes, no comparison with the NACA series has been conducted. Additionally, some parameters were not examined such as different tip speed ratio (TSR), solidity (σ), and pitch angle (β). R.A. Ghazalla et al. [10] used a wind lens for studying conventional NACA0015 and DU-06-W-200 airfoils in addition to non-conventional J-shape blades. They concluded that J-shape airfoils have a better power coefficient compared to NACA0015 and DU-06-W-200. Jain and Saha [11] presented a 2D incompressible numerical investigation of the impact

of thickness to chord ratio of various NACA symmetrical airfoils on the dynamic stall in a single-bladed rotor H-type Darrieus VAWT at a single operating point (TSR = 2.0). The selected thickness-to-chord ratios were 9%, 12%, 15%, 18%, and 21%. They found that for thinner airfoils, laminar separation bubbles (LSBs) lead to a leading-edge dynamic stall while there were LSBs at the thicker airfoils trailing edge. W. Tjiu et al. [12] proposed to improve the aerodynamic performance of the VAWT by substituting airfoils typically employed in the NACA series with more widely utilized HAWT airfoils, such as the NLF and hybrid NLFNACA 4 series. The Darrieus VAWT's unique design was introduced in the study. Takahashi et al. [13] demonstrated a numerical simulation using direct numerical simulation (DNS) that is based on the finite difference method in addition to an experimental wind tunnel test by “wind lens” to study the performance of various airfoils for straight-bladed vertical axis wind turbine (SB-VAWT). For the DNS results, symmetrical airfoils are more efficient than un-symmetrical ones. Based on the wind tunnel, NACA0024 has the best performance. The findings showed that the SB-VAWT with a wind lens can achieve a power augmentation of more than two. M. Jason et al. [14] analyzed ten various NACA airfoils, five of them were of symmetrical type and the rest were non-symmetrical type through 2D CFD simulation to get the suitable airfoil aerodynamically for a certain VAWT. A parametric study was performed including the variation of TSRs, ranging from 2.2 to 8.2, at a constant entering wind velocity, of 8 m/s. The study reveals that the symmetrical NACA airfoil, specifically NACA0018 had the most efficient performance while NACA0010 provided the lowest power coefficient. Nevertheless, for non-symmetrical airfoils, NACA2421 recorded the highest power coefficient. M. Tirandaz et al. [15] demonstrated an optimal design analysis of a series of symmetric NACA airfoils based on their thickness, chordwise position, and leading-edge radius for a single-rotor VAWT using a morphing airfoil technique at low TSR. Enormously intensive 2D, incompressible, and unsteady CFD simulations are performed for these airfoils at two distinct TSRs (2.5, 3.0) where a dynamic stall exists. The impact of other airfoil series, such as S-profile, as well as cambered NACA airfoils on the optimal design, however, was not discussed in the study. Additionally, Investigation of the study for a wide range of TSRs is not demonstrated. The study recommended studying the effect of other parameters on the turbine performance such as turbine solidity (i.e., turbine blade numbers), Reynolds number, and turbulence intensity, besides studying the blade structural loads' effect on the turbine performance along with the aerodynamic loads.

All the previous literature works provided valuable attempts to improve the aerodynamic performance of the VAWT from different points of view whether the study was numerical or experimental or both. Most of the publications examined symmetrical NACA00XX airfoils [7-15] while a few of them studied cambered or non-symmetrical NACA airfoils [7, 14]. The S-profile airfoil category is analyzed through a few papers [7-9]. In addition, few researchers examined the Delft airfoil category [10]. Few publications used a hybrid HAWT and NACA airfoil.[12]. Moreover, no prior literature has ever featured the Eppler profile. Furthermore, several research publications recommended more examination of distinct types of airfoils performance and the development of new optimized airfoils. According to the previous short-term discussion about the complex phenomena at low-Reynolds number flow and in the light of previous publications gaps, it is essential to study the enhancement of the aerodynamic performance of low-Re airfoils implemented in H-rotor Darrieus VAWT.

This paper presents a comparative study of the aerodynamic performance of various VAWT blade low-Reynolds number airfoils to determine the best shape that can be utilized for various flow

regimes. Three different categorized symmetric airfoils—NACA0021, Eppler474, and S1048—, as well as three cambered airfoils— NACA6712, S1210, and DU-06-W-200—, have been chosen to be examined throughout this paper. These airfoils are suitable for implementation in the wind turbines at low Reynolds number [3].

2. Reference model study

A three-bladed H-rotor straight vertical axis wind turbine (VAWT) presented by Castelli et al. [16] is used as a reference model to be validated and verified against available experimental and numerical data. The main geometrical specifications of the used model are exhibited in **Table 1**.

Table 1. Main geometrical features of the examined VAWT model [16]

Parameter	**Description**
VAWT type	Straight bladed Darrius
Number of blades *N*	3
Blade airfoil profile	NACA0021
Blade airfoil chord *c*	0.0858 m
Rotor diameter Drotor	1.03 m
Solidity $\sigma = 2N\ c/D_{rotor}$	0.5
Rotor height H	Unity for 2D simulation
Spoke blade connection	0.25 *c*
Installed power	~ 0.2 kW

2.1. Governing equations and turbulence model selection

The Unsteady Reynolds Averaged Navier Stokes URANS equation considering the turbulence spectrum in the flow is solved using an adequate turbulence model. The URANS equation accompanied by the continuity equation is used to characterize 2D, incompressible, viscous, and isothermal flow. The present study solves 2D, unsteady, incompressible, and viscous flow. The solution of this flow field is performed numerically using a high-fidelity CFD software package, ANSYS Fluent 18.0. The governing equations are the mass conservation and momentum equations.

The mass conservation can be written in Einstein notation (tensor form) as:

$$\frac{\partial u_i}{\partial x_i} = 0 \tag{1}$$

Where ui represents the velocity field in three dimensions, xi represents the coordinates in 3 dimensions and i = 1,2,3.

For Newtonian fluid, the URANS can be written as:

$$\rho\frac{\partial u_i}{\partial x_i} + \rho u_j\frac{\partial u_i}{\partial x_j} = -\frac{\partial p}{\partial x_i} + \mu\frac{\partial}{\partial x_j}\left(\frac{\partial u_i}{\partial x_j} + \frac{\partial u_j}{\partial x_i}\right) + \frac{\partial}{\partial x_j}\left(-\rho\overline{u_i' u_j'}\right) \tag{2}$$

where ρ is the fluid density, p is the pressure, μ is the dynamic viscosity, and $-\rho\overline{u_i' u_j'}$ represents the Reynolds stress [17]. According to the literature, the suitable turbulence model used to describe the

flow at a low Reynolds number is the SST-k-ω. This model is composed of two equations: the "k" equation characterizes the turbulent kinetic energy in the flow, while the "ω" equation represents the flow's specific rate of dissipation (3) and (4).

$$\frac{\partial k}{\partial t} + U_i \frac{\partial k}{\partial x_i} = \frac{\partial}{\partial x_i}\left[(\nu + \sigma_k \nu_t)\frac{\partial k}{\partial x_i}\right] + P_k - C_\mu \omega k \tag{3}$$

$$\frac{\partial \omega}{\partial t} + U_i \frac{\partial \omega}{\partial x_i} = \frac{\partial}{\partial x_i}\left[(\nu + \sigma_\omega \nu_t)\frac{\partial \omega}{\partial x_i}\right] + \gamma \frac{\omega}{k} P_k - \beta \omega^2 + (1 - F_1)\frac{2\sigma_\omega}{\omega}\frac{\partial k}{\partial x_i}\frac{\partial \omega}{\partial x_i} \tag{4}$$

The SST-k-ω model is described in detail in [18-20].

2.2. Computational domain analysis

2D rectangular mixed structured and unstructured cells are generated by Pointwise 18.3R2 meshing software. The computational domain consists of a rotating domain that describes the turbine rotor and a stationary domain that mimics the flow field. **Fig. 1** exhibits the main characteristics of the computational domain besides the used boundary conditions.

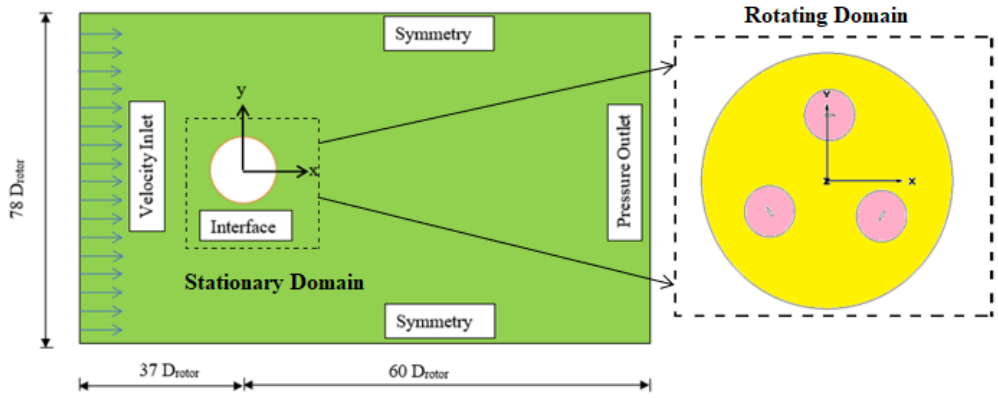

Fig. 1. A schematic drawing of stationary and rotating domains with specified boundary conditions (not to scale)

It is crucial to perform the mesh independence study to select the suitable and stable mesh for the reference case study and further simulations. Different meshes depending on various airfoil surface discretization have been examined at a tip speed ratio of 2.63 which corresponds to the maximum power coefficient. **Fig. 2** shows that the power coefficient value becomes stable around 0.5 million cells. Further discretization results in insignificant accuracy in the power coefficient. Thus, 0.5 million cells have been selected to be utilized for all simulations throughout the study.

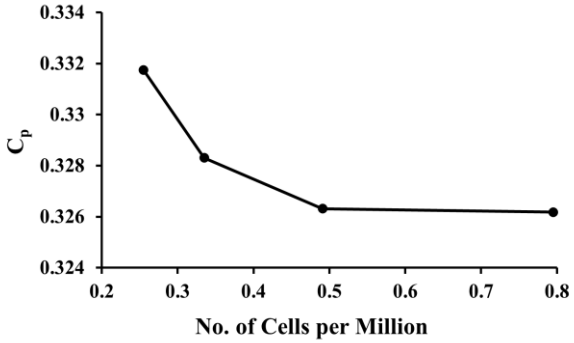

Fig. 2. Mesh Independence Test

The generated computational domain meshing is shown in **Fig. 3**. The total number of cells is about 305,000 triangular cells and 185,500 quad cells. The structured grids are used around the airfoils while the unstructured ones are used in the remaining domain. Furthermore, the cells around the domain containing the airfoils are intensified by creating control circles. The control circle dimension is about 1.5 times the airfoil chord while the rotating domain dimensions are about 2 times the turbine rotor diameter. To develop a more precise solution, 512 points are used in discretizing the airfoil's upper and lower surfaces. To decrease the vortices at the trailing edge of the airfoil, a half-circle is used instead of a blunt or sharp trailing edge. Additionally, an inflation of about 20 layers with an average growth rate of 1.05 (the growth rate represents the increase in element edge length with each succeeding layer of elements from the edge or face), and the height of the first cell was about 0.03 mm which corresponds to y+~1 (y+ is a non-dimensional distance measures whereas the mesh was coarse or fine) is created around the airfoil surface to capture the boundary layer accurately [19]. Furthermore, the mesh refinement surrounding the airfoil is depicted in **Fig. 3**.

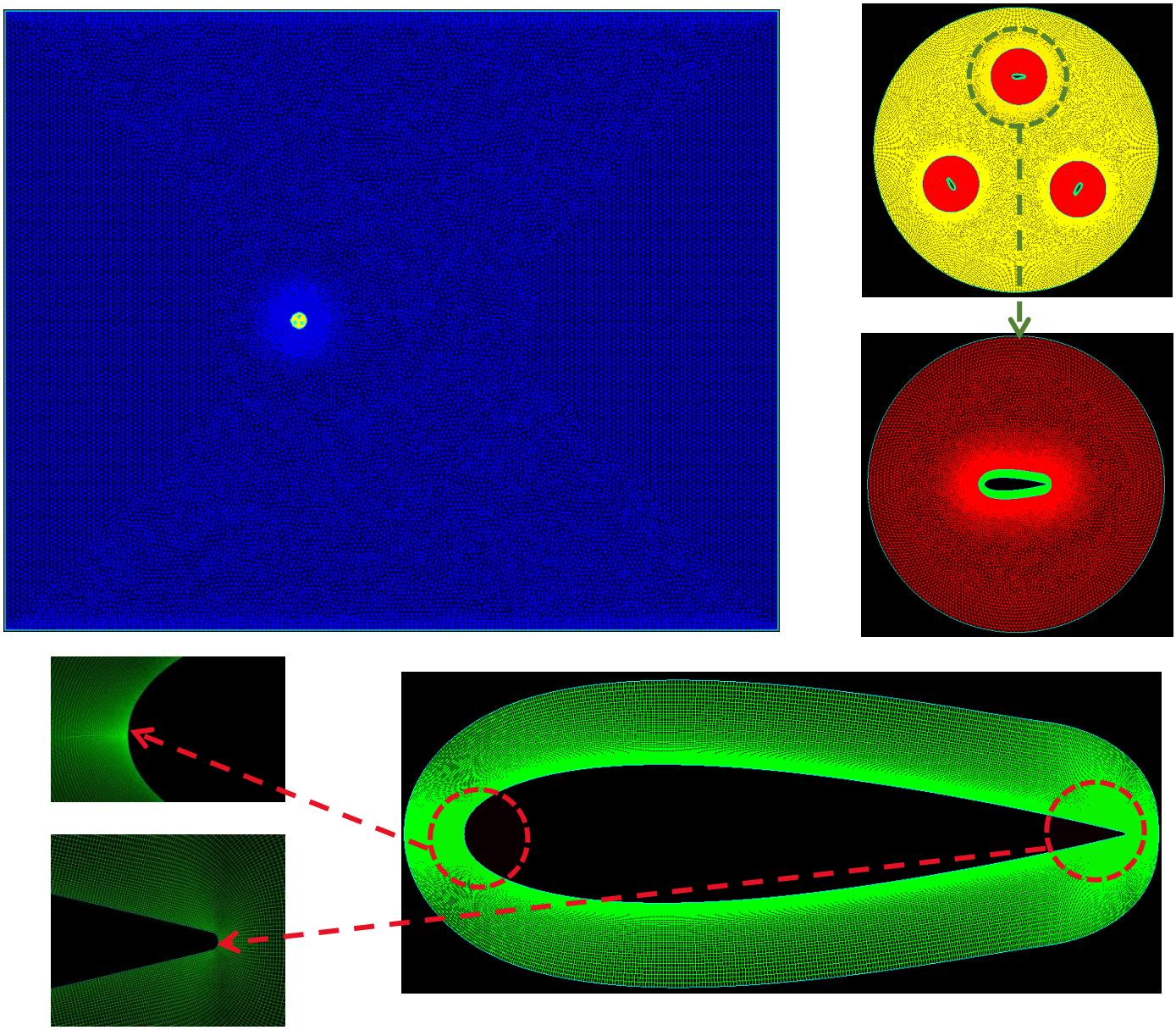

Fig. 3. Meshing distribution for the stationary domain (left), rotating domain (right), and around the NACA0021 airfoil (down)

2.3. Performance parameters definitions

The main performance parameters are the tip speed ratio (TSR, λ), the power coefficient (C_P), and the torque coefficient (C_T). They can be defined as follows:

$$TSR = \lambda = \frac{\omega D_{rotor}}{2U_\infty} \tag{5}$$

$$C_P = \frac{T\omega}{0.5\,\rho U_\infty^3 H\,D} \tag{6}$$

$$C_T = \frac{T}{0.25\rho U_\infty^2 H D^2} \tag{7}$$

The Tip-speed ratio is defined as the ratio between the tangential speed of the tip of a blade and the actual speed of the wind while the power coefficient is defined as the ratio between the power

produced by the wind and the total power available by the wind. Its maximum limit is about 0.593 which corresponds to the Betz limit [21].

The power coefficient and the torque coefficient can be related by inserting the tip speed ratio definition as follows:

$$C_P = C_T \lambda \tag{8}$$

Where ω, T, U_∞, H, D_{rotor}, and ρ are the angular velocity VAWT, applied torque, free stream velocity (wind speed), rotor blade height, rotor blade diameter, and the air density, respectively.

Furthermore, the chordal Reynolds number (Re) and solidity (σ), can be defined, and used throughout the study as follows:

$$\overline{Re_c} = \frac{\rho U_\infty c}{\mu} \tag{9}$$

$$\sigma = \frac{2\,Nc}{D_{rotor}} \tag{10}$$

where $\overline{Re_c}$ is the mean chordal Reynolds number, μ is the freestream air dynamic viscosity, N is the number of turbine blades, and c is the blade airfoil chord.

The azimuth angle is defined as the angle measured counterclockwise from the turbine rotor vertical axis that is perpendicular to the wind speed direction as in **Fig. 4**.

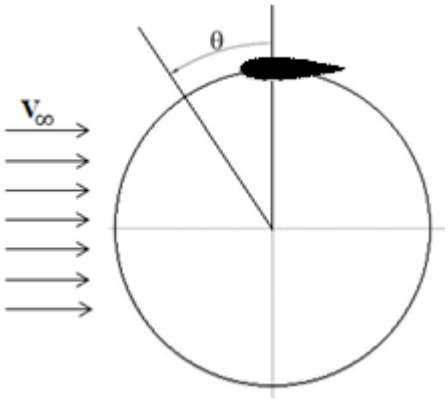

Fig. 4. Azimuth angle (θ) definition.

2.4. Solver computational settings

The numerical simulations are performed using Pointwise 18.3 R2 as a meshing tool and commercial CFD package ANSYS Fluent V18.0 to solve a 2D, incompressible unsteady viscous flow by solving the URANS (unsteady Reynolds-Averaged Navier-Stokes) equation using the sliding mesh (SM) technique [22]. The selected turbulence model is SST-k-ω, all with second-order schemes for spatial and temporal discretization. The Semi-Implicit Method for Pressure Linked Equations, SIMPLE, scheme is used for coupling the velocity and pressure fields [16, 23]. Utilizing the time step Δt that corresponds to 1° azimuth angle increment (Δθ = 1°) is an appropriate value for the simulations and further decreasing this time step does not provide a significant effect on the solution [24].

The time step and the azimuth angle are related as follows:

$$\Delta t = \frac{\Delta\theta^{\circ}}{6n} \tag{11}$$

Where n is the rotational speed in rpm

Furthermore, all calculations are performed at a constant inlet air velocity of 9 m/s and a Re ≅ 50,000 based on the airfoil chord. **Table 2** presents more details about the simulation settings.

Table 2. Simulation Parameters

Parameter	Description
TSR, λ	Varying (1.2 →4.0)
Free stream velocity U∞	9 m/s
Rotational speed (N)	Varying (200→650 rpm)
Solver type	Pressure-based
Flow type	Unsteady, transient
Solution algorithm	SIMPLE
Turbulence model	SST-k-ω
Residuals	1e-4 for all equations 1e-5 for the momentum equation
Unsteady technique	Sliding Mesh
Fluid (Air)	Incompressible, ρ = 1.225 kg/m3, μ = 1.7894e-5 kg/m/s
Boundary conditions	*Inlet*: uniform velocity inlet (9 m/s) *Outlet*: pressure outlet *Sides*: symmetry *Rotor interface*: interface *Blades*: Wall with no slip – rotational relative to the adjacent domain.
Reference values	A = D H = 1.03 m^2 L = D/2 = 0.515 m V = 9 m/s H = 1 m ρ = 1.225 kg/m^3 μ = 1.7894e-5 kg/m/s

2.5. Convergence criteria

If the difference in the average torque coefficient between two successive revolutions is less than 1%, the simulation is converged. That occurs at complete revolutions ranging from 8→20 revolutions relative to the operation conditions. Furthermore, the acceptable range for the residuals convergency is 10^{-4} for the mass conservation equation and turbulence model variables and 10^{-5} for the momentum conservation equations.

2.6. Reference model verification and validation

The CFD numerical simulation of the reference model (NACA0021) for various tip-speed ratios is demonstrated to validate the results against both publicly available experimental data and published CFD simulation [16]. The present reference model provides a decent concurrence with the available published experimental data than the used literature CFD simulation (**Fig. 5**). Moreover, the maximum percentage error in the power coefficient between the present reference model and the experimental data is less than 5%. This small error percentage comes from that the experiment setup did not include the effect of the wind tunnel blockage [16], consequently, the experimental results appeared to be approximately 2D analysis rather than 3D analysis. The reference model NACA0021 provides a maximum power coefficient of about 0.3263 at TSR = 2.63. **Fig. 6** clarifies the convergence of the power coefficient C_P against the number of revolutions at $\lambda = 2.63$. It is observed that, after the 6th revolution, the variation of average C_P is not significant, and the percentage error has dropped by 1%.

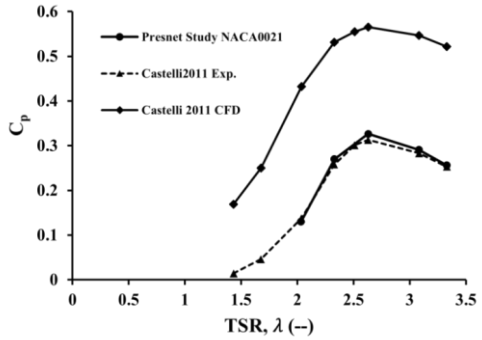

Fig. 5. Reference model (NACA0021) validation and verification

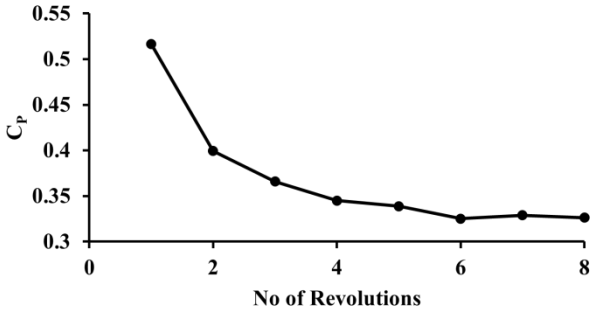

Fig. 6. Variation of average C_P at TSR = 2.63 for 8 successive revolutions (Reference model)

3. RESULTS AND DISCUSSION

The same turbine model and computational settings are used for various blade airfoil shapes that have the same chord length. They are NACA6712, S1210, DU-06-W-200, Eppler474, and S1048. These airfoils are an appropriate solution to be implemented in wind turbines operating at low Reynolds numbers [3].

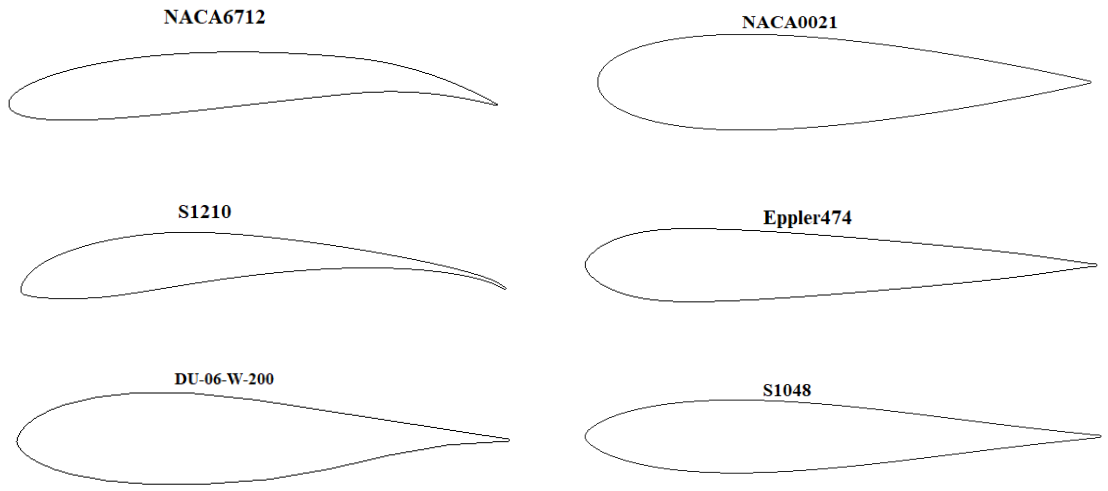

Fig. 7. List of proposed blade airfoils (cambered airfoils on the left and symmetric airfoils on the right)

The reference model (NACA0021) airfoil, as well as the proposed airfoils, are exhibited in **Fig. 7**. The power coefficient at different tip-speed ratios of the studied airfoil profiles as well as the instantaneous torque developed over the turbine rotor circumference are demonstrated. Additionally, the maximum power coefficient and its corresponding tip-speed ratio are presented for the studied airfoils. Consequently, the selection of the proper airfoil for various flow regimes is carried out.

3.1. Symmetric airfoils

For symmetric airfoils, **Fig. 8** provides the power coefficient variation at different rotational speeds, TSRs, for the studied symmetric airfoils (NACA0021, Eppler474, and S1048). Eppler474 airfoil type has the maximum power coefficient along almost all TSR ranges. It experienced an enhancement of the power coefficient than the reference model one by about 9% at TSR = 3.0. Additionally, the Eppler474 airfoil possesses about 2% improvement in the power coefficient than the reference model, but at a higher TSR (λ = 3.3). This is due to the enlarged thickness of the reference model more than the other two profiles at the expected separation zone near the trailing edge. On the other hand, the S1048 has a 2% enhancement in the maximum power coefficient at TSR = 3.3 relative to the reference model. At further TSR, specifically at TSR = 3.89, the S1048 airfoil produces approximately the same reference model power coefficient. This is again due to the difference in the rate of decreasing the profile thickness of the two profiles at the ends, and due to the increased speed leading to moving the maximum value in the direction of flow towards the end. Moreover, compared to the reference model at the same tip-speed ratio (TSR = 2.033), the S1048 exhibits a notable improvement in the maximum power coefficient which is approximately 33% of the C_P has improved due to the gradient decrease of the thickness.

The instantaneous torque distribution over the turbine rotor azimuth angle at the TSRs corresponding to the maximum power for the symmetric airfoils is presented in **Fig. 9**. The Eppler474 airfoil is the superior airfoil performed at the upstream region (θ from 0→180°) and its maximum torque coefficient occurs at about $\theta \cong 101°$ that shifted than the reference model, NACA0021, by about 4°. While in the downstream region (θ from 180→360°), the instantaneous torque remains almost constant but has a value lower than the reference model one. Then again,

the S1048 airfoil possesses a decent torque distribution in the upstream region, and it occurs at θ ≅ 98° shifted than the reference model by about 1°. For the downstream region, the S1048 airfoil has an instantaneous torque distribution lower than both the reference model and the Eppler474 airfoil.

3.2. Cambered airfoils

For cambered airfoils, **Fig. 10** exhibits the power coefficient variation at different TSRs, i.e. different rotor rotational speeds, for the proposed cambered airfoils (NACA6712, DU-06-W-200, and S1210). The DU-06-W-200 airfoil performs efficiently for almost all TSR ranges, specifically for higher TSR regions (from 2 to 3.5). Its maximum power coefficient occurs at TSR = 3.0 and it has a percentage improvement relative to the reference model of about 4%. Over and above, the DU-06-W-200 airfoil experienced a nearly constant power coefficient at TSR = 3.3 relative to the reference model value that occurs at TSR = 3.0. That resulted in developing the same power coefficient but at a rotational speed larger than that of the reference model. This is obviously due to the improvement of the circulation around the trailing edge because of the camber decreasing at the end of the profile. The S1210 airfoil has a reasonable power coefficient variation along the almost TSR range. However, it experiences an approximately constant power coefficient at TSR = 3.6 relative to the reference model at TSR = 3.0 In addition, it possesses a percentage improvement of the power coefficient at TSR = 2 by about 30%. The NACA6712 airfoil behaves more efficiently than the other airfoils at low rotational speeds, i.e., low TSRs (1.2→2.4), due to the lesser circulation at lower speeds. The NACA6712 airfoil possesses a maximum power coefficient enhanced by about 12% at TSR = 2.0 relative to the reference model (TSR = 2.63). Additionally, for lower TSR, TSR = 1.2 for example, it provides a power coefficient enhancement percentage of about 9% rather than the reference model at TSR = 2.033. Nevertheless, the NACA6712 performs deficiently at TSRs larger than 2.4. The instantaneous torque distribution over the turbine rotor azimuth angle at the TSRs corresponding to the maximum power for the cambered airfoils is presented (**Fig. 11**).

The NACA6712 airfoil exhibits superior torque distribution for both upstream and downstream regions at TSR = 2. Both of S1210 and DU-06-W200 airfoils have almost the same torque distribution in the upstream region but the DU-06-W200 experienced more efficient torque distribution in the downstream region at TSR = 3 rather than the S1210 airfoil at TSR = 3.3, however, the changes are not in general significant.

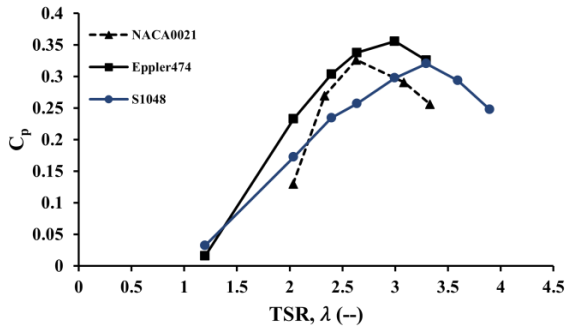

Fig. 8. Turbine power coefficient for different TSRs (Symmetric airfoils)

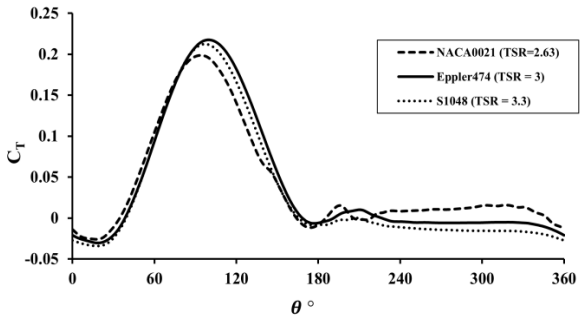

Fig. 9. Instantaneous torque distribution over the wind turbine rotor revolution (Symmetric airfoils)

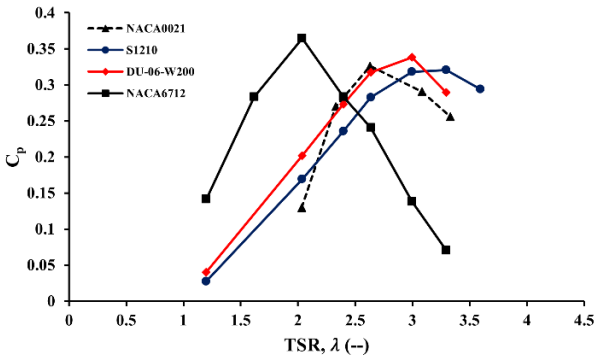

Fig. 10. Turbine power coefficient for different TSRs (Cambered airfoils)

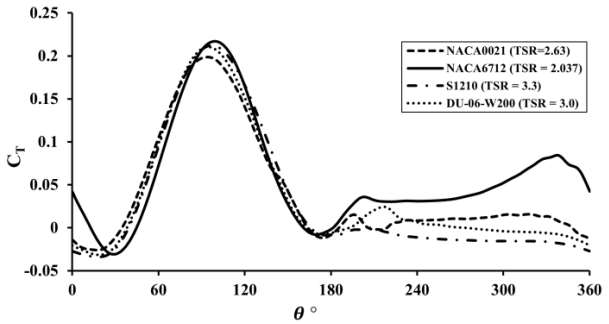

Fig. 11. Instantaneous torque distribution over the wind turbine rotor revolution (Cambered airfoils)

3.3. Comparative analysis

Fig. 12 provides various proposed airfoil shapes maximum power coefficient and the corresponding TSR. It is clarified that the NACA6712 airfoil has the maximum power coefficient (C_P = 0.36452), at a relatively low TSR (2.037) while, the Eppler474 airfoil provides the maximum power coefficient (C_P = 0.35566) at a relatively large TSR (3.0). Conversely, the S1210 and S1048 airfoils have the lowest maximum power coefficient ($C_P \cong 0.32$) at TSR = 3.3.

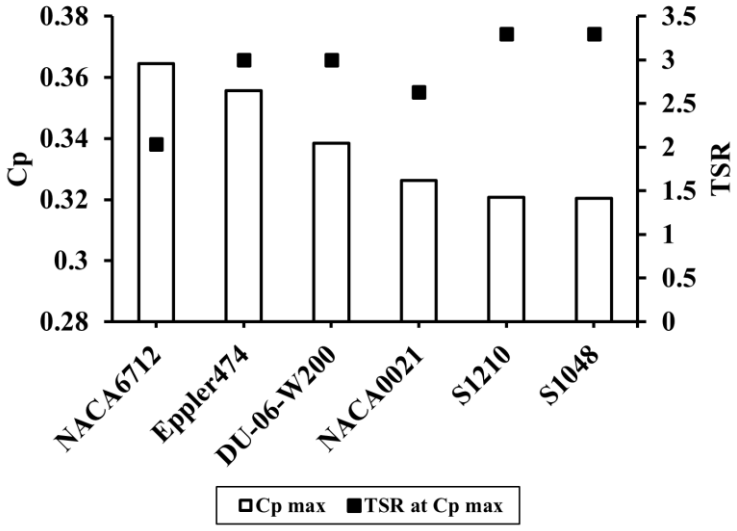

Fig. 12. Proposed airfoil shapes maximum power coefficient and corresponding TSR

Conclusions

The paper presented a qualitative and quantitative comparative analysis of the aerodynamic performance of low Reynolds number airfoils to provide a road map for utilizing an appropriate wind turbine blade airfoil for various flow regimes that correspond to the maximum power coefficient. Distinct types of airfoils of a certain straight-bladed Darrieus wind turbine were examined through 2D numerical simulations to determine whether the airfoil has the best aerodynamic performance at different flow regimes. The proposed airfoils were NACA0021, Eppler474, S1048, NACA6712, DU-06-W200, and S1210.

The results revealed that the NACA6712 airfoil has the best aerodynamic performance at low TSR ranges (1.2→2.4). At TSR = 2.0, its improvement was about 9% in the power coefficient compared to the reference model NACA0021 airfoil at TSR = 2.63, however, its performance decreased as the TSR was larger than 2.4. For the high TSR regime, the Eppler474 airfoil was the appropriate airfoil, and it has an enhancement in the power coefficient of about 9% at TSR = 3.0 relative to the reference model, NACA0021 airfoil. Accordingly, the paper recommended utilizing the NACA6712 airfoil in the low relative wind speed regions (TSRs from 1.2→2.4) and the Eppler474 airfoil in the high relative wind speed regions (TSRs from 2.0 to 4.0) for a straight-bladed Darrieus wind turbine.

References

[1] O. Ozgener and L. Ozgener, "Exergy and reliability analysis of wind turbine systems: A case study," Renewable and Sustainable Energy Reviews, vol. 11, no. 8. pp. 1811–1826, 2007.

[2] M. Ahmad, A. Shahzad, and M. N. M. Qadri, "An overview of aerodynamic performance analysis of vertical axis wind turbines," Energy-and-Environment, 2022.

[3] S. J. Miley, "Catalog of low-Reynolds-number airfoil data for wind-turbine applications." 1982.

[4] B. H. Carmichael, "Low Reynolds number airfoil survey," NASA-CB-165803, vol. 1, no. November, 1985.

[5] H. P. Horton, "Laminar separation bubbles in two and three-dimensional incompressible flow.," PhD, London Univ., 1968.

[6] M. Abul-Ela and M. M. Abdelrahman, "Numerical Simulation of 2D Tandem Wing at Low Reynolds Number using Parametric Study," in 14th International Conference of Fluid Dynamics, 2-3 April 2021, Fairmont Nile City Hotel, Cairo, EGYPT, 2021, no. ICFD14-EG-7059, pp. 1–13.

[7] T. Tahzib, M. A. Hannan, Y. A. Ahmed, I. Zamil, and M. Kamal, "Performance Analysis of H-Darrieus Wind Turbine with NACA0018 and S1046 Aerofoils : Impact of Blade Angle and TSR," CFD Lett., vol. 2, no. 2, pp. 10–23, 2022.

[8] S. Roy and H. Branger, "2017-ASME-DESIGN OF AN OFFSHORE THREE-BLADED VERTICAL AXIS WIND TURBINE FOR WIND TUNNEL EXPERIMENTS," in Proceedings of the ASME 2017 36th International Conference on Ocean, Offshore and Arctic Engineering OMAE2017 June 25-30, 2017, Trondheim, Norway D, 2017.

[9] I. . Hashem and M. H. Mohamed, "Aerodynamic Performance Enhancements of H-rotor Darrieus Wind Turbine," Energy, 2017.

[10] R. A. Ghazalla, M. H. Mohamed, and A. A. Hafiz, "Synergistic analysis of a Darrieus wind turbine using computational fluid dynamics," Energy, vol. 189. 2019.

[11] S. Jain and U. K. Saha, "On the influence of blade thickness-to-chord ratio on dynamic stall phenomenon in H-type Darrieus wind rotors," Energy Convers. Manag., vol. 218, 2020.

[12] W. Tjiu, T. Marnoto, S. Mat, M. H. Ruslan, and K. Sopian, "Darrieus vertical axis wind turbine for power generation II: Challenges in HAWT and the opportunity of multi-megawatt Darrieus VAWT development," Renew. Energy, vol. 75, pp. 560–571, 2015.

[13] S. Takahashi, Y. Ohya, T. Karasudani, and K. Watanabe, "Numerical and experimental studies of airfoils suitable for Vertical Axis Wind Turbines and an application of wind-energy collecting structure for higher performance," in 4th International Symposium on Computational Wing Engineering (CWE2006), Yokohama,2006.

[14] M. Jason et al., "2D CFD Simulation Study on the Performance of Various NACA Airfoils," vol. 4, no. 4, pp. 38–50, 2021.

[15] M. R. Tirandaz and A. Rezaeiha, "Effect of airfoil shape on power performance of vertical

axis wind turbines in dynamic stall : Symmetric Airfoils," Renew. Energy, vol. 173, pp. 422–441, 2021.
[16] M. Raciti Castelli, A. Englaro, and E. Benini, "The Darrieus wind turbine: Proposal for a new performance prediction model based on CFD," Energy, vol. 36, no. 8, pp. 4919–4934, 2011.
[17] Fluent Software, "Modeling Turbulent Flows," 2001.
[18] S. M. A. Aftab, A. S. M. Rafie, N. A. Razak, and K. A. Ahmad, "Turbulence Model Selection for Low Reynolds Number Flows," pp. 1–15, 2016.
[19] R. H. Nichols, "Turbulence Models and Their Application to Complex Flows," no. August, 2008.
[20] J. Wauters and J. Degroote, "On the study of transitional low-Reynolds number flows over airfoils operating at high angles of attack and their prediction using transitional turbulence models," Prog. Aerosp. Sci., vol. 103, pp. 52–68, Nov. 2018.
[21] Z. Lubosny, Wind Turbine Operation in Electric Power Systems. 2003.
[22] Fluent Software, "ANSYS FLUENT User ' s Guide," 2010.
[23] F. Trivellato and M. R. Castelli, "On the Courant e Friedrichs e Lewy criterion of rotating grids in 2D vertical-axis wind turbine analysis," Renew. Energy, vol. 62, pp. 53–62, 2014.
[24] M. R. Castelli, G. Ardizzon, L. Battisti, E. Benini, and G. Pavesi, "Modeling strategy and numerical validation for a Darrieus vertical axis micro-wind turbine," ASME Int. Mech. Eng. Congr. Expo. Proc., vol. 7, no. PARTS A AND B, pp. 409–418, 2010.